

Neutron and X-ray Tomography (NeXT) system for simultaneous, dual modality tomography

J. M. LaManna*, D. S. Hussey*, E. Baltic*, D. L. Jacobson*

* Physical Measurement Laboratory, National Institute of Standards and Technology, Gaithersburg, MD, USA

Abstract:

Dual mode tomography using neutrons and X-rays offers the potential of improved estimation of the composition of a sample from the complementary interaction of the two probes with the sample. We have developed a simultaneous neutron and 90 keV X-ray tomography system that is well-suited to the study of porous media systems such as fuel cells, concrete, unconventional reservoir geologies, limestones, and other geological media. We present the characteristic performance of both the neutron and X-ray modalities. We illustrate the use of the simultaneous acquisition through improved phase identification in a concrete core.

Introduction:

Tomography is a widely utilized non-destructive method to determine the structure of complex samples. As shown by Liu¹, the use of a second probe that has a different cross section, enables a more accurate estimation of the composition of the interrogated sample. One field of study that is of interest is porous media in which one typically wishes to observe the distribution of a hydrogenous material within a mineral matrix. For these materials, the combination of X-ray and neutron imaging is advantageous, as X-rays have good sensitivity for the matrix, while neutrons have good sensitivity for the hydrogenous components. This is owing to the fact that X-rays primarily interact with material through the electron cloud while neutrons primarily interact with material through the strong nuclear force. This is shown in Figure 1 where the attenuation coefficients for thermal neutrons and 90 keV X-rays^{2,3} is given, which highlights large differences in attenuation for various materials such as hydrogen and iron. Thus, by combining the image data sets from both probes, a more complete understanding of a multi-phase sample can be obtained. This leads to a more straightforward segmentation of various materials to improve structural or flow models.

Typically, neutron and X-ray imaging would be implemented in a serial configuration where the sample would be imaged with one technique followed by the other⁴⁻¹¹. Problems arise when investigating samples that slowly evolve with time or stochastic processes as samples will not be identical for each imaging mode as scans can take around 12 h to 24 h or more to complete, so only average information can be extracted from the data. To overcome these issues while facilitating improved material identification and volume registration, simultaneous, dual-mode, neutron and X-ray imaging is necessary. An X-ray generator can be placed perpendicular to the neutron beam so that the sample sits at the intersection of the beams. The first example of a system like this was implemented by Sinha et al. at the Missouri University of Science and Technology Reactor¹²⁻¹⁵. This system demonstrated the benefits of combining neutron and X-ray imaging but was limited in spatial resolution and application by the power of the reactor. A new simultaneous system is also under development at the Imaging with Cold Neutrons (ICON) beamline at the Swiss Spallation Neutron Source (Spallations Neutronen Quelle, SINQ) at the Paul Scherrer Institut¹⁶.

We report on a system for simultaneous neutron and X-ray imaging that has been developed and installed at the National Institute of Standards and Technology (NIST) Center for Neutron Research thermal neutron imaging facility. This work will describe the neutron and X-ray system components and operation and give an example application, the examination of concrete, that benefits from dual-mode imaging.

2. Experimental setup

2.1 Overview of NeXT system

The NeXT (Neutron and X-ray Tomography) system operates by orienting a microfocus X-ray tube perpendicular to the neutron beam. Samples sit at the intersection of the two beams as shown in Figure 2. This orientation provides simple registration of the two tomograms by rotating the X-ray volume by 90° to align with the neutron volume. The engineering model shown in Figure 2 gives the layout of the beam directions (neutron beam shown in red and X-ray beam shown in blue) and detector placement for each beam.

2.2 Details of the NIST thermal neutron imaging facility

The NIST thermal neutron imaging facility is located on the beam tube 2 (BT2) thermal neutron port at the NIST Center for Neutron Research. This facility provides an intense beam of thermal neutrons for imaging research from a 20 MW nuclear fission reactor. A schematic layout of the instrument is given in Figure 3. Thermal neutrons exit the reactor vessel through an aluminum beam port tube called the thimble and are initially collimated by a tapered tube consisting of steel rings with progressively smaller internal diameters labeled #2 in Figure 3. This produces a conical beam with near uniform intensity. Although the beam is primarily thermal neutrons, higher energy neutrons and gamma rays from the reactor are present in the beam and could be detrimental to sensor electronics and pose a radiation safety concern. A liquid nitrogen cooled bismuth filter, 10 cm in length, (#3 in Figure 3) is used to remove these unwanted beam components. The 10 cm Bi filter reduces the thermal neutron fluence rate by about a factor of four.

Neutron image geometric unsharpness, λ_g , and fluence rate are controlled with the aperture assembly (#4 in Figure 3). The aperture assembly provides selectable pinhole sizes to control the L/D (collimation) ratio where L is the distance from the pinhole to the detector and D is the diameter of the pinhole. With a sample to detector distance given by z, $\lambda_g = z D/L$. Larger values of L/D provide greater collimation and sharper images for large z, but at the expense of the thermal neutron fluence rate which scales as $(D/L)^2$. There are two sample positions available inside the BT2 enclosure. The most commonly used sample position is at the 6 m position where the beam is about 26 cm in diameter with a maximum fluence rate of $3 \times 10^7 \text{ cm}^{-2} \text{ s}^{-1}$. The shorter, 3 m position is used when the test requires a factor 4 higher neutron fluence rate (on the order of $10^8 \text{ cm}^{-2} \text{ s}^{-1}$) with a 13 cm beam diameter and small L/D ratios. L/D ratios at BT2 range from 150 when high intensity is needed, to 6 000 when high resolution is needed. The NeXT system sits at the 6 m position and typically employs a 1 cm aperture with a fluence rate of $6 \times 10^6 \text{ cm}^{-2} \text{ s}^{-1}$.

A rotating drum of heavy concrete is located just downstream of the aperture assembly and serves both as a local shutter control and additional background reduction. The drum has four positions, 1 closed

and 3 open, that allow control of beam state and amount of background reduction. Position 1 is the closed, solid concrete position that stops the beam to allow access to the instrument enclosure. Positions 2 to 4 are open tubes with different internal diameters that provide increasing amounts of collimation to reduce background gamma rays and fast neutrons. A fast acting thermal neutron shutter constructed from two 1 mm thick sheets of cadmium backed by two 6.5 mm thick sheets of borated aluminum is positioned after the drum. This shutter provides uniform illumination for image plates and allows the fast neutron and gamma contribution to the image to be measured as the thicknesses of Cd and B minimally attenuate fast neutrons or gammas. After the fast shutter, the neutrons enter an evacuated flight tube with 2 mm thick aluminum windows that transport the neutrons from the local shutter to the sample position. The tube is kept under rough vacuum to reduce the neutron attenuation due to interaction with air, about a 3 % reduction per meter. The entire system is situated inside a shielded enclosure that contains the high radiation fields present from the beam and sample activation. Steel shot and wax inside the shield walls absorb scattered neutrons and gamma rays emitted from the sample and equipment inside the enclosure.

2.3 Details on the X-ray imaging system

The X-ray imaging system consists of an X-ray generator, beam conditioning equipment, and detector system. X-rays are generated with an Oxford Instruments UltraBright microfocus X-ray generator¹⁷ which produces a cone beam with cone angle of about 35 degrees. This device has a 10 μm to 20 μm spot size (at maximum voltage and minimum power) and operates with a voltage range of 20 kV to 90 kV and maximum current of 2 mA. At maximum power, the X-ray generator produces a continuous Bremsstrahlung spectrum from approximately 15 keV to 90 keV with tungsten characteristic peaks at 59 keV and 67 keV. This produces a mean energy of approximately 32 keV that can be raised with the addition of filtration to block out the lower energy X-rays from the Bremsstrahlung continuum. A tungsten slit system is positioned just downstream of the X-ray generator to control the size of the beam at the sample and to prevent direct X-ray exposure to the neutron detector. By removing the unneeded beam to the side of the sample with the tungsten mask the sample can be placed in close proximity to the neutron detector. The X-ray generator and detector are mounted on linear rails to allow for movement in the beam axis direction so that flight path length, field of view (FOV), and geometric magnification can be adjusted. A heat sink mounted to the front face of the X-ray generator ensures that the temperature of the X-ray generator remains below 45 °C which strongly reduces drift in the X-ray spot location.

The linear stages on which the X-ray generator and detector are mounted allow for variable source to sample distance (Z_x) and source-to-detector distance (L_x) as shown in Figure 4. These distances control the photon flux on the sample and the geometric magnification of the sample, $M = L_x/Z_x$, on the detector due to the divergence of the generated cone beam. Higher geometric magnification allows greater spatial resolution to be achieved for a given intrinsic detector spatial resolution. The available X-ray detector FOV limits the maximum magnification as the object being imaged must fit within the FOV.

2.4 Detectors and image characteristics

imaging detectors used for both neutron and X-ray modalities use Gadolinium Oxysulfide (GadOx) scintillators viewed by a camera¹⁸, as shown in Figure 5. A mirror at 45° to the primary beam is used to reflect the scintillation light at a 90° angle to keep the camera electronics out of the primary beam to prevent radiation damage. Light produced by the scintillator screen is focused onto the camera using standard Nikon lenses. Currently available lenses include a 50 mm f1.2, 85 mm f1.4, 105 mm f2.8, 200 mm f4, and extension tubes to alter the reproduction ratio of the 85 mm lens. This permits optimizing the image resolution and field of view for the sample under study by selecting the appropriate lens. The cameras used for both detectors are Andor NEO scientific complementary metal-oxide-semiconductor (sCMOS) cameras with a 2560x2160 pixel chip with 6.5 μm pixel pitch. Effective pixel size and FOV specifications for various lens configurations are given in Table 1.

Data acquisition software developed in-house allows for the simultaneous control of both cameras and the 6-axis sample motion control system to maintain time correlation between imaging modes. The two cameras can operate at different frame rates and number of accumulated frames to optimize image statistics for each mode. Temporal resolution is typically set by the neutron imaging system due to the inherently lower fluence rate of the neutron beam compared to the X-ray system. The sample rotation stage indexes to the next projection angle once both detectors have completed the user-specified exposure time and number of images. Projection angles can be acquired sequentially or with custom, user-specified positions, such as those employed for quasi-dynamic systems using the golden ratio method¹⁹.

There is a potential for a systematic background in either the neutron or X-ray detector due to scattering of the complementary beam since the same GadOx scintillator material is used in both detectors. To eliminate this potential systematic, each detector is shielded from the opposite beam. The neutron detector has a 6 mm thick lead sheet placed between the sample and the scintillator face to block any scattered X-rays from causing erroneous neutron signal; the neutron transmission through 6 mm of lead is about 99 %. A 3.5 mm thick sheet of lithiated polyethylene is placed between the sample and the X-ray detector to absorb the scattered neutron beam without emission of a gamma ray; the X-ray transmission through the 3.5 mm of lithiated plastic at the peak spectrum energy of 90 keV with 4 mm of aluminum filtration is 95 %. In both cases, the measured background from the other modality is identical to the offset image with no radiation present.

2.5 Sample vessel material considerations for NeXT imaging

Many types of systems require some form of containment cell to facilitate fluid flow under pressure, isolation from atmosphere, temperature control, etc. Choice of material for the sample cell is critical for the simultaneous neutron and X-ray imaging setup to minimize the attenuation of each beam as much as possible. Mass attenuation coefficients are given in Table 2 for several common engineering materials used in X-ray or neutron imaging. The mass attenuation coefficients for X-ray are given for 45 keV X-rays which represents the mean energy of the X-ray generator when operating at the typically used 90 keV peak energy with 2 mm of aluminum filtration. Typically, in X-ray imaging it is desirable to use low atomic weight, that is low Z, materials to reduce the attenuation of the beam since attenuation increases with increasing Z. Materials usually chosen include beryllium and plastics such as polyethylene. Neutrons on the other hand require materials with no hydrogen content and can easily penetrate metals such as aluminum and steel. Because of the large neutron scattering cross-section for hydrogen,

Polymers are preferred where plastic and elastomer materials are required. As shown in Table 2, most metals such as steel have a large cross-section for X-rays while hydrogenated polymers like polyethylene have a very large cross-section for neutrons. In summary, the optimal material selection for sample vessels for NeXT are magnesium, aluminum, carbon and polytetrafluoroethylene (PTFE). NIST has designed a pressure vessel from aluminum to investigate pressurized flow at moderate temperatures in geological specimens that will be detailed in a future manuscript.

3 Identification of degradation modes in concrete using NeXT System

Concrete is a multiphase system with several degradation modes that can lead to premature and unexpected failure of critical infrastructure such as buildings and bridges. One important degradation mode is delayed ettringite formation (DEF) where the brittle mineral ettringite crystallizes in voids and cracks along aggregate-paste interfaces in hardened concrete. Due to the hydrogen content of ettringite, determining the distribution throughout a sample of concrete lends itself to neutron tomography. X-rays provide additional information on structure such as the paste-aggregate interfaces and voids within the paste. In prior efforts, researchers interested in using both neutron and X-ray tomography to analyze concrete must use different facilities for each mode like a reactor or spallation source for neutrons or a lab based X-ray scanner or synchrotron radiation facility and data sets can be separated in time by some weeks. This is problematic for the analysis of the onset of DEF as significant changes and expansion of the concrete can occur over this time period. Applying the NIST NeXT system, the evolution of DEF can be accurately tracked with excellent volume registration between the modes to allow more reliable estimates of compositional changes in core samples up to 5 cm in diameter. By combining the two modes it is also possible to make two-dimensional histograms (neutron vs. X-ray attenuation coefficients) of the material allowing for greater separation between individual material peaks. The greater separation of peaks is necessary to properly identify and distinguish ettringite from water as they have similar neutron attenuation coefficients but different X-ray mass attenuation coefficients.

The differences in attenuation between neutrons and X-rays produces contrast differences that highlight various features within the concrete as shown in Figure 6. Voids that appear very strongly in the X-ray image are often difficult to differentiate from the surrounding material in the neutron image. This indicates that what appears to be a gas filled void in the X-ray is actually a water/liquid filled pore from the neutron data. Information regarding the pores/voids present in the concrete matrix would be missed by only using a single imaging mode whereas the simultaneous system gives the full picture. The state of these voids can change with time as the water is absorbed/redistributed as the concrete hydrates and cures. Figure 7 shows how the X-ray reconstruction highlights interfacial effects compared to just the neutron image alone. The arrow highlights a crack along an aggregate which has formed from the cement paste separating and pulling away. This is a prime region for the future growth of ettringite which is indicated as brighter spots in that region in the neutron image.

Current efforts on data reduction and material identification are ongoing. Reconstruction techniques and alignment algorithms are being improved to better overlay the volumes and identify individual materials. High resolution imaging of the concrete core samples with a focused ion beam – scanning

Electron microscope will provide validation of the mineral structure in the regions identified by the neutron tomography reconstruction. Concrete samples with intentionally engineered composition variation are currently being imaged over several months to collect a time sequence for identifying the onset and growth of DEF.

4 Conclusions

A simultaneous neutron and X-ray tomography system has been established at NIST. Simultaneous tomography is accomplished by placing a microfocus X-ray generator perpendicular to a neutron beam. The sample sits at the intersection of the two beams and each transmission image is captured by separate detectors. Crosstalk between the modes has been mitigated through the use of shielding that is transparent for the desired beam while opaque to the opposite beam. The system offers significant benefits over serial imaging: capturing dynamic or stochastic systems with each mode in identical states, offering complementary information arising from the differences in material interaction with the two modes, faster overall acquisitions times, and simplified volume alignment. The system has proven useful for a range of applications including fuel cells, batteries, petrogeology, and concrete. An example from concrete demonstrated the ability to improve the detection of flaws and defects in materials that would have been missed by single mode imaging. The improvement in material phase detection and separation will allow understanding to the formation of unwanted phases and improvements to the strength and durability of concrete.

Acknowledgments

This work was supported by the U.S. Department of Commerce, the NIST Radiation and Physics Division, the Director's office of NIST, and the NIST Center for Neutron Research. The authors would like to thank Professor Richard Livingston of The University of Maryland for providing the concrete samples used in this work.

¹X. Liu, L. Yu, A. N. Primak and C. H. McCollough, *Med Phys* 36, 1602 (2009).

²M. J. Berger, J. H. Hubbell, S. M. Seltzer, J. Chang, J. S. Coursey, R. Sukumar, D. S. Zucker and K. Olsen, <http://physics.nist.gov/xcom>, (2010).

³P. Kienzle, Scattering Length Calculator, <https://www.ncnr.nist.gov/resources/activation/>.

⁴M. Balaskó, F. Kőrösi and Z. Szalay, *Appl. Radiat. Isot.* 61, 511 (2004).

⁵J. Dewanckele, T. De Kock, G. Fronteau, H. Derluyn, P. Vontobel, M. Dierick, L. Van Hoorebeke, P. Jacobs and V. Cnudde, *Mater. Charact.* 88, 86 (2014).

⁶D. Mannes, C. Benoît, D. Heinzelmann and E. Lehmann, *Archaeometry* 56, 717 (2014).

⁷D. Mannes, E. Lehmann, P. Cherubini and P. Niemz, *Trees* 21, 605 (2007).

⁸M. J. Schrapp, M. Goldammer, M. Schulz, S. Issani, S. Bhamidipati and P. Böni, *J. Appl. Phys.* 116, 163104 (2014).

⁹E. Solórzano, S. Pardo-Alonso, N. Kardjilov, I. Manke, F. Wieder, F. García-Moreno and M. A. Rodríguez-Perez, *Nucl. Instrum. Methods Phys. Res. B* 324, 29 (2014).

¹⁰R. Triolo, G. Giambona, F. Lo Celso, I. Ruffo, N. Kardjilov, A. Hilger, I. Manke and A. Paulke, *Conserv. Sci. Cultural Heritage* 10, 143 (2010).

¹¹T. A. Waigh and C. Rau, *Curr. Opin. Colloid Interface Sci.* 17, 13 (2012).

¹²V. Sinha, Ph.D. Dissertation, Missouri University of Science and Technology, 2013.

¹³V. Sinha, A. Srivastava and H. Koo Lee, *Nucl. Instrum. Methods Phys. Res. A* 750, 43 (2014).

¹⁴V. Sinha, A. Srivastava, H. Koo Lee and X. Liu, *Nucl. Instrum. Methods Phys. Res. A* 750, 12 (2014).

¹⁵V. Sinha, A. Srivastava, H. K. Lee and X. Liu, *Proceedings of SPIE* 8694, 86940R-2 (2013).

¹⁶A. Kaestner, D. Mannes, J. Hovind, P. Boillat and E. Lehmann, *Proceedings of 6th Conference on Industrial Computed Tomography*, 1 (2015),

http://www.ndt.net/article/ctc2016/papers/ICT2016_paper_id13.pdf.

¹⁷Certain trade names and company products are mentioned in the text or identified in an illustration in order to adequately specify the experimental procedure and equipment used. In no case does such identification imply recommendation or endorsement by the National Institute of Standards and Technology, nor does it imply that the products are necessarily the best available for the purpose.

¹⁸A. Koch, *Nucl. Instrum. Methods Phys. Res. A* 348, 654 (1994).

¹⁹A. Kaestner, B. Münch, P. Trtik and L. Butler, *Opt. Eng* 50, 123201 (2011).

ACCEPTED MANUSCRIPT

Table 1: Detector effective pixel pitch and FOV specifications

| pixel size [μm] | Field of View [mm] |
|-----------------|--------------------|
| 6.5 | 17 X 14 |
| 9.0 | 23 X 19 |
| 10.5 | 27 X 23 |
| 15.0 | 38 X 32 |
| 17.2 | 44 X 37 |
| 23.9 | 61 X 52 |
| 30.0 | 77 X 65 |
| 51.4 | 131 X 111 |

ACCEPTED MANUSCRIPT

Table 2: Mass attenuation coefficients for common engineering materials typically used for sample environment.

| Material | Density [g cm ⁻³] | Mass Attenuation Coefficient [cm ² g ⁻¹] | |
|---------------------------|----------------------------------|--|---------------------|
| | | 45 keV x-ray | Thermal neutrons |
| Beryllium | 1.848 | 0.15920 | 0.510254 |
| Carbon | 1.7 | 0.19570 | 0.371101 |
| Magnesium | 1.74 | 0.39150 | 0.09274 |
| Aluminum 6061 | 2.699 | 0.54480 | 0.038782 |
| Titanium | 4.54 | 1.57800 | 0.126975 |
| 304 Stainless Steel | 7.874 | 2.58100 | 0.153068 |
| Inconel 625 | 8.44 | 4.34600 | 0.193839 |
| Copper | 8.96 | 3.49800 | 0.110971 |
| Polytetrafluoroethylene | 2.25 | 0.22640 | 0.162667 |
| High Density Polyethylene | 0.96 | 0.20690 | 6.908333 |

ACCEPTED MANUSCRIPT

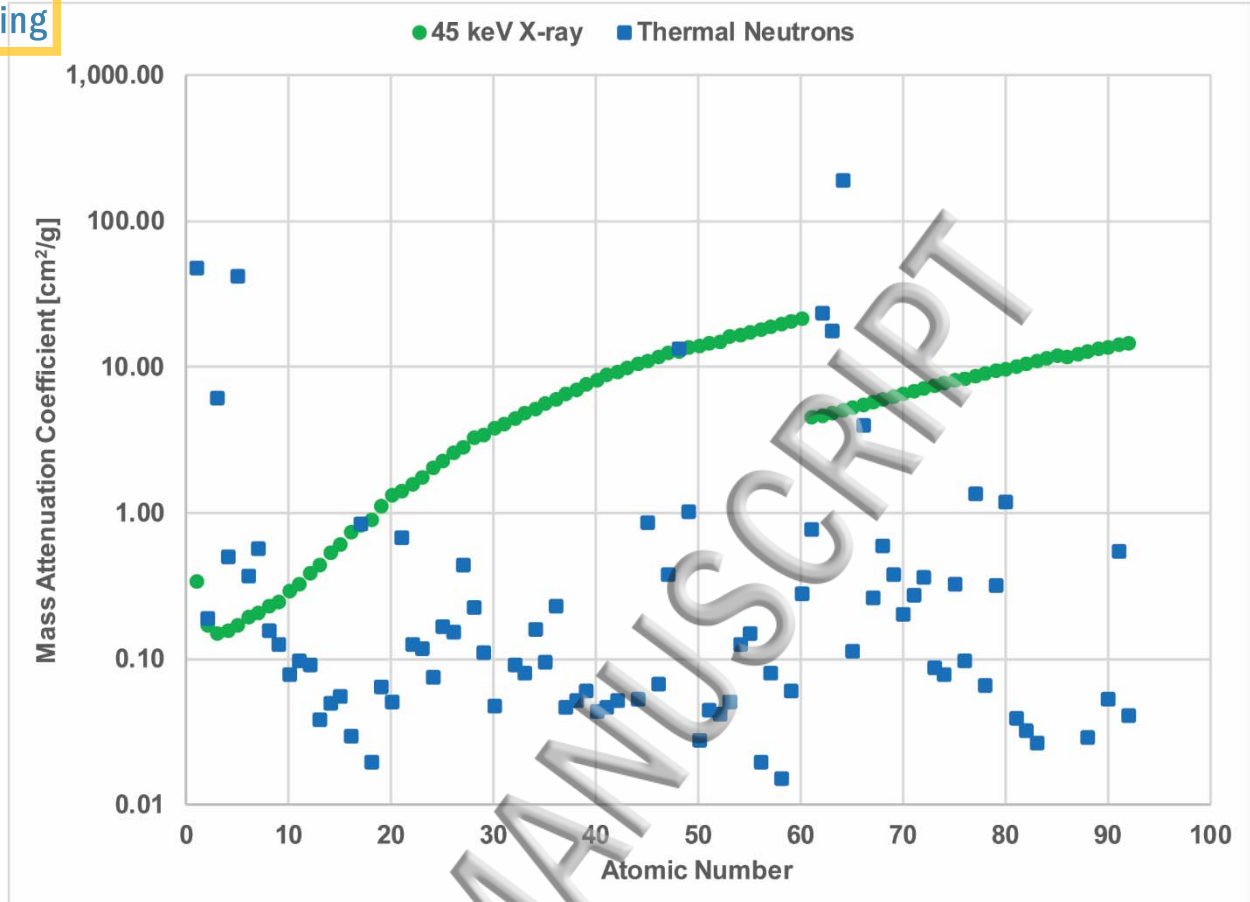


Figure 1: Comparison of 90 keV X-ray and thermal neutron (25 meV) mass attenuation coefficients as a function of atomic number, where the neutron cross section assumes natural isotopic abundances.

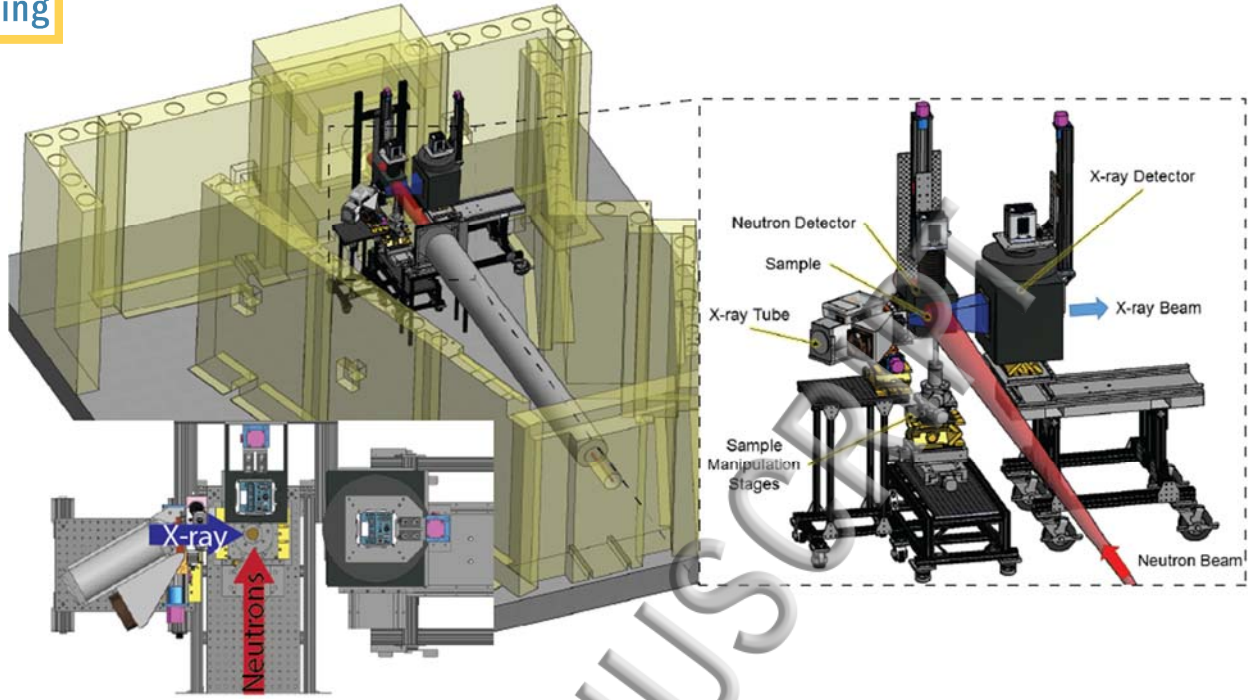


Figure 2: Engineering model representation of NeXT system with neutron beam in red and X-ray beam in blue. Enclosure roof panels have been removed for clarity.

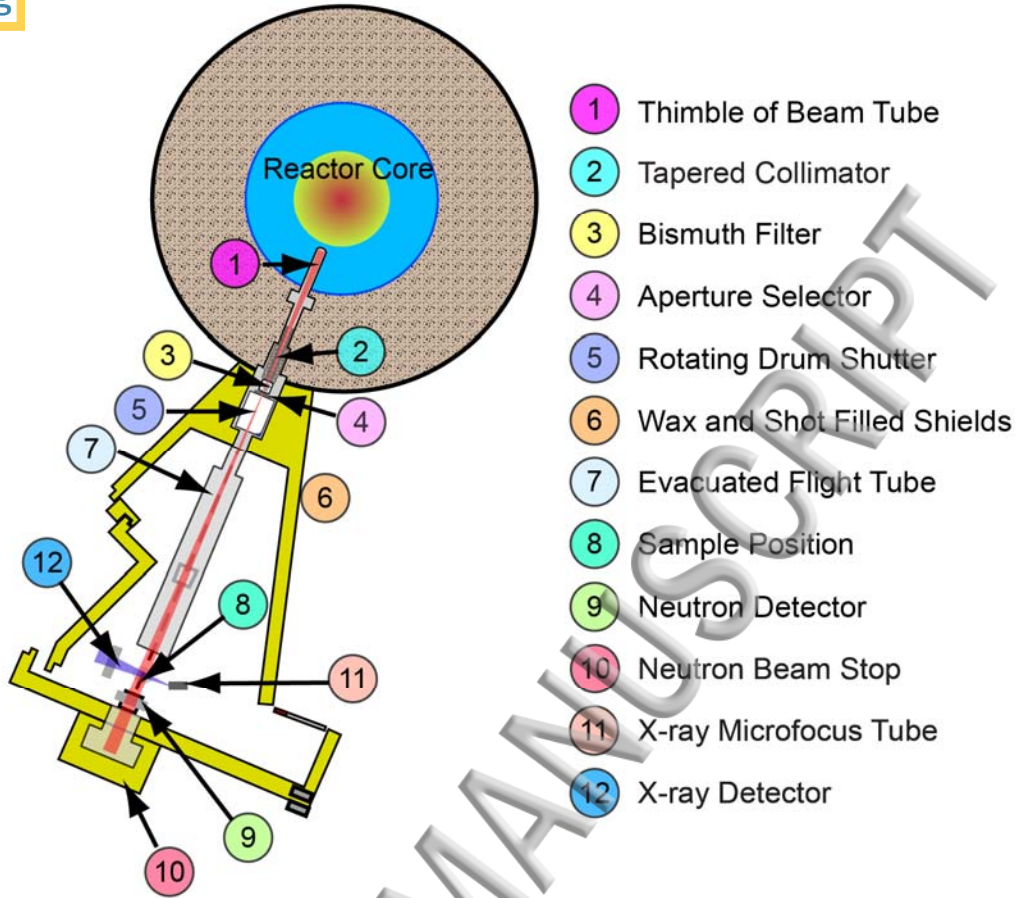


Figure 3: Schematic layout of the neutron imaging facility.

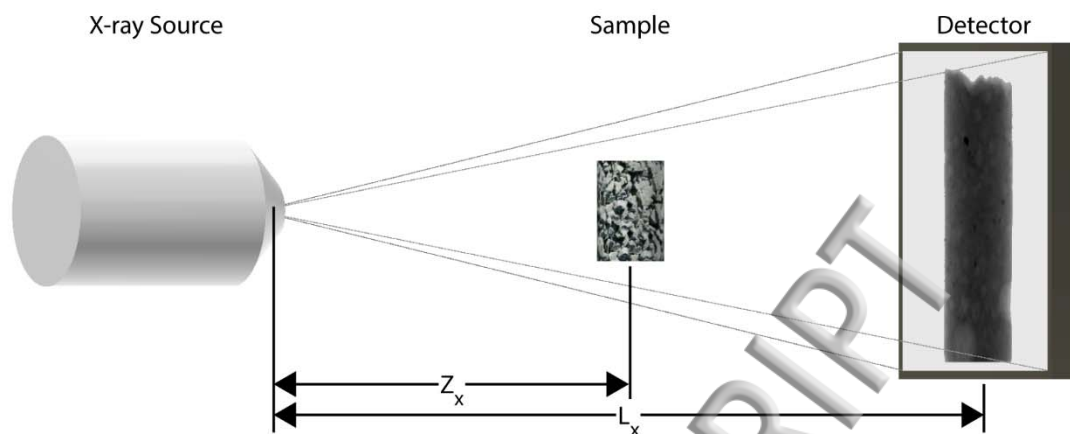


Figure 4: Schematic overview of X-ray imaging system dimensions.

ACCEPTED MANUSCRIPT

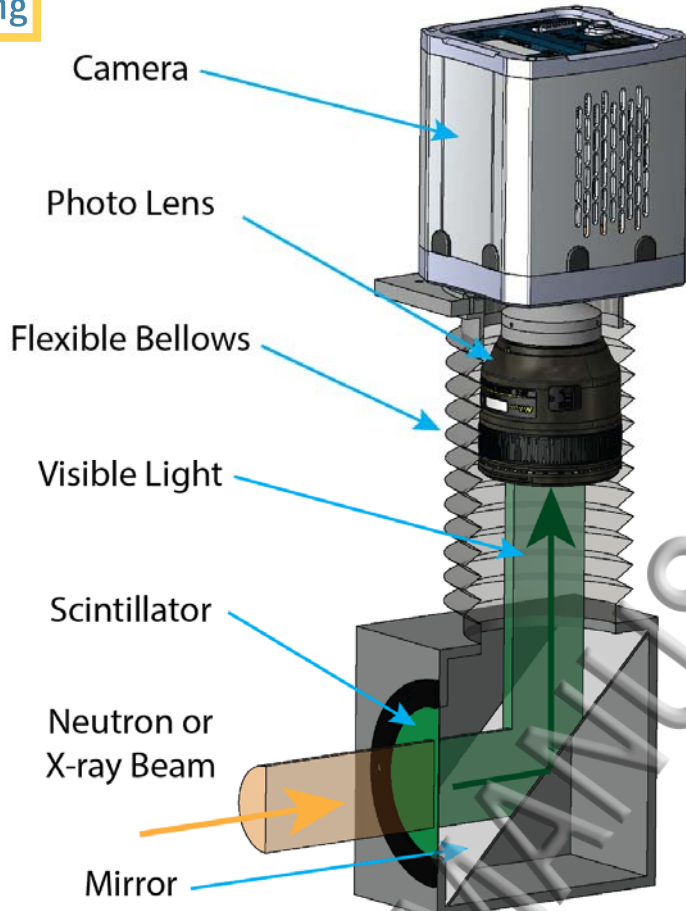


Figure 5: Schematic layout of neutron and X-ray detectors.

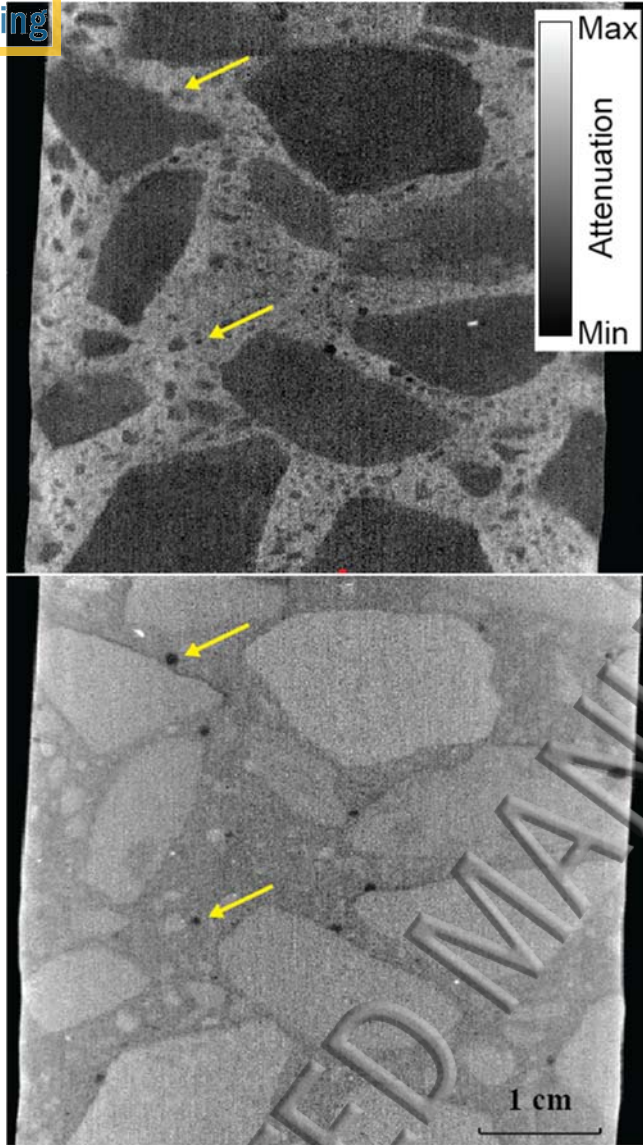


Figure 6: Grayscale cross-sectional slices showing contrast differences between neutron (top) and X-ray (bottom). Voids marked with the arrow in the X-ray can be difficult to distinguish in the neutron image suggesting that the void is partially water filled.

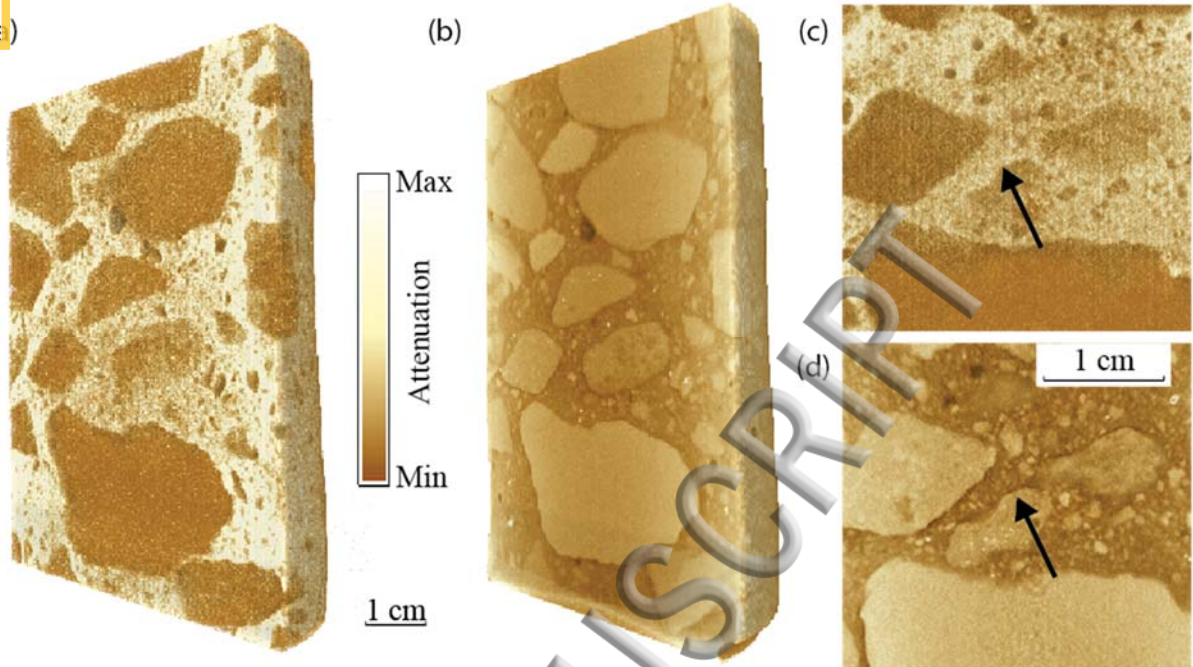
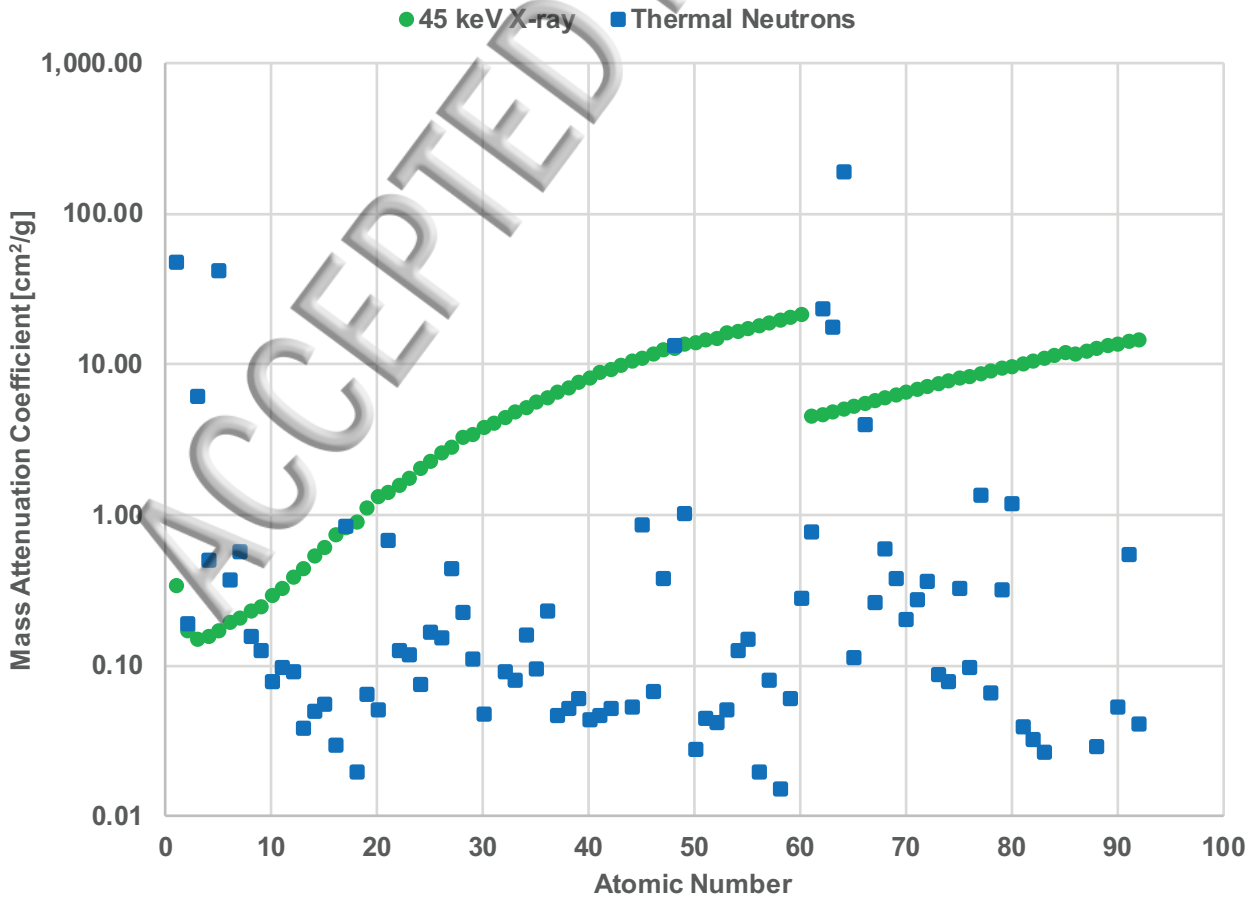
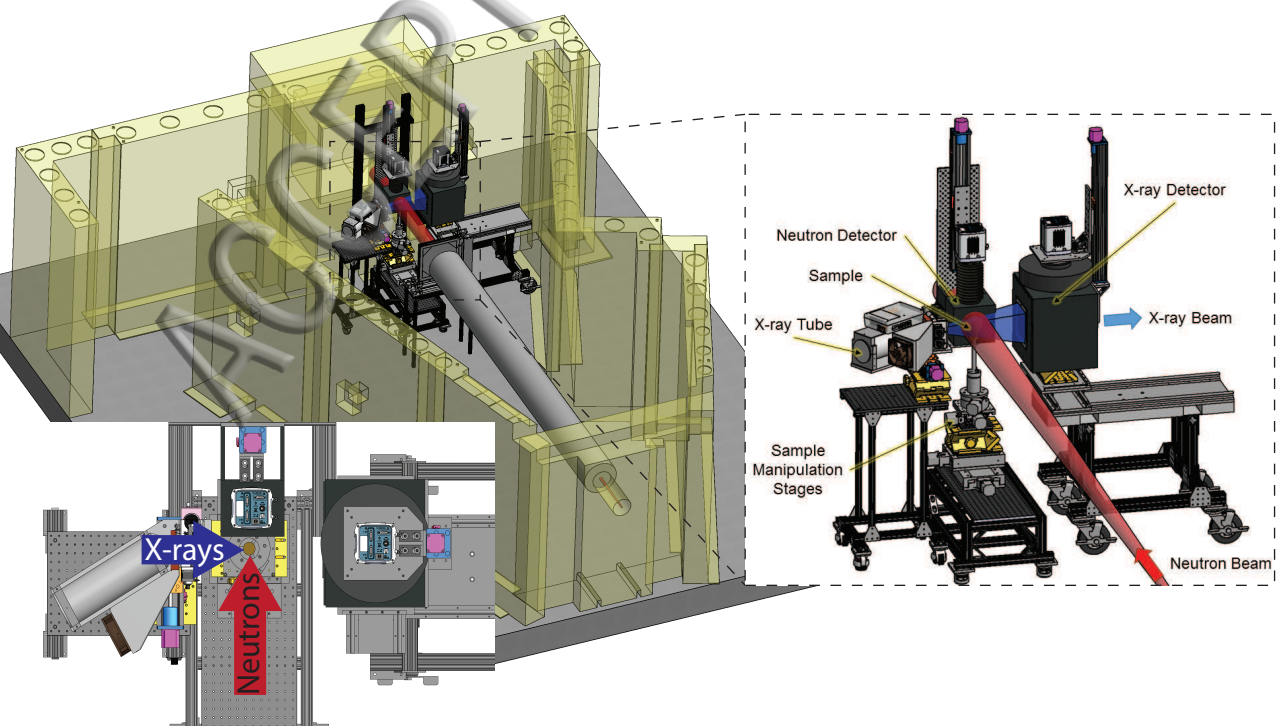
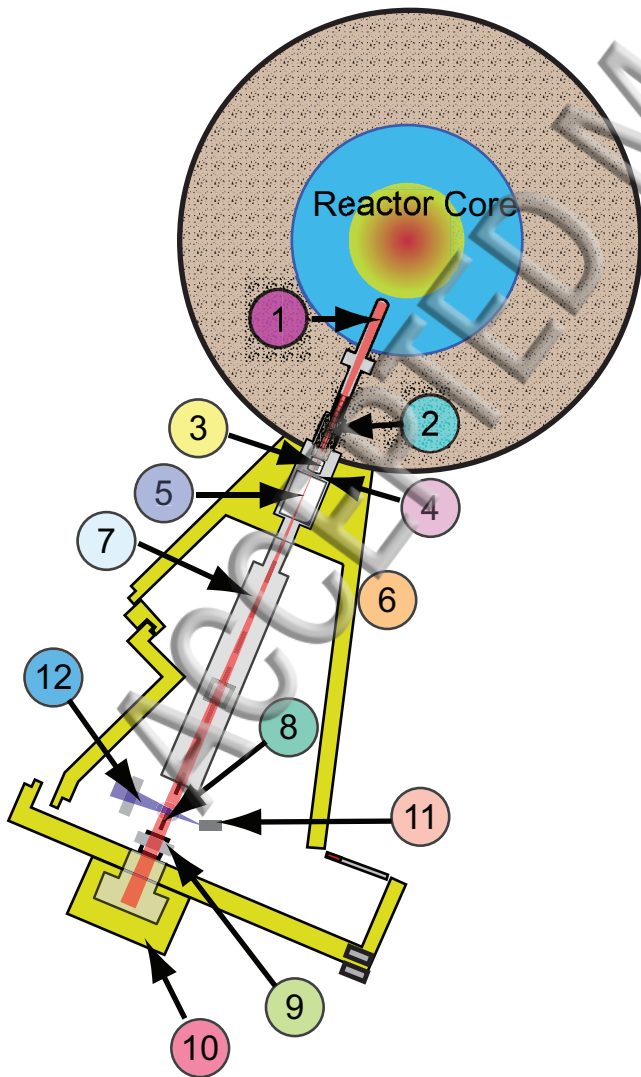


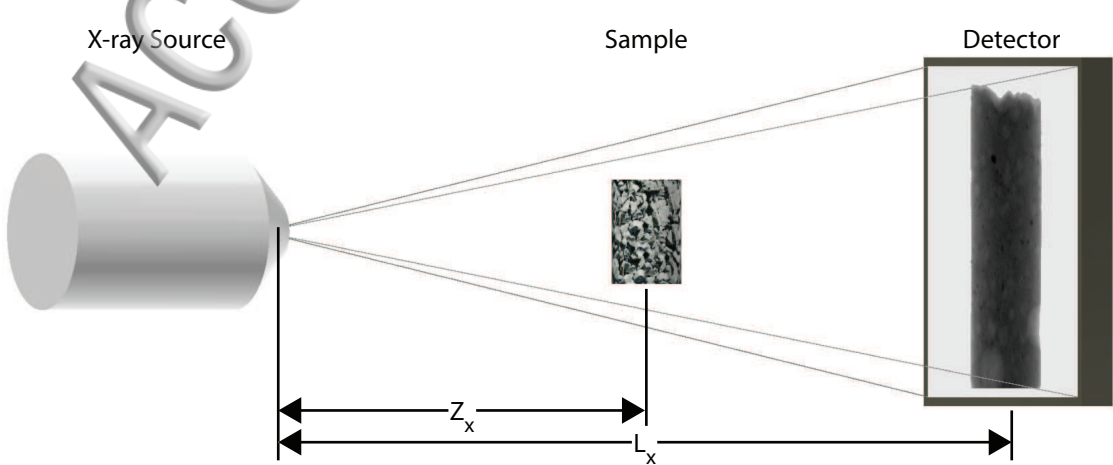
Figure 7: 3-D volume renderings of the tomographic reconstructions of concrete (neutrons (a), X-rays (b)) and central slices showing a region of interest (neutron (c), X-ray (d)). Arrows indicate paste/aggregate separation in the X-ray image and corresponding bright areas in the neutron image indicating possible presence of ettringite.

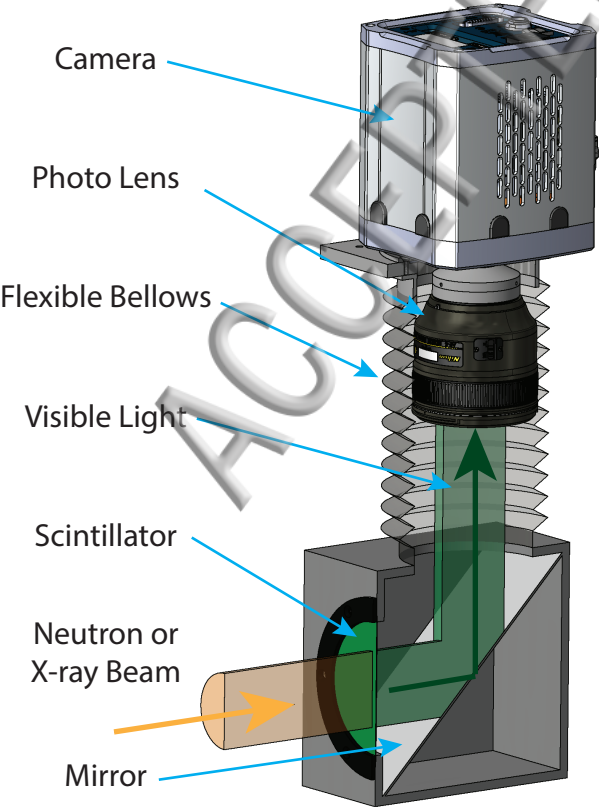


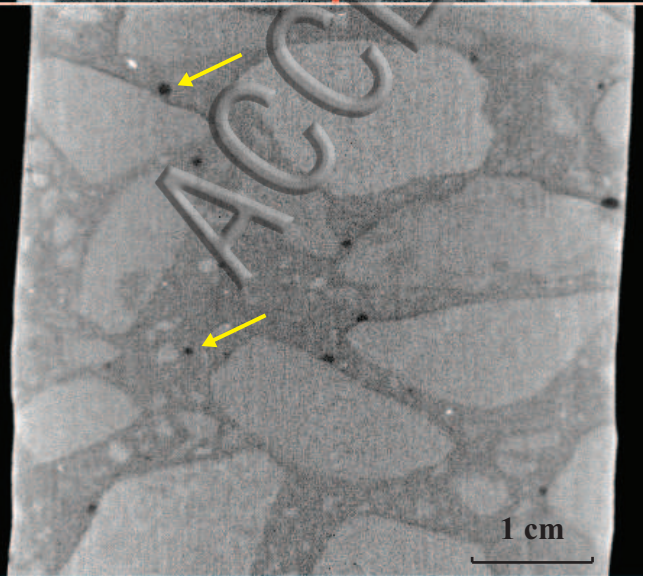
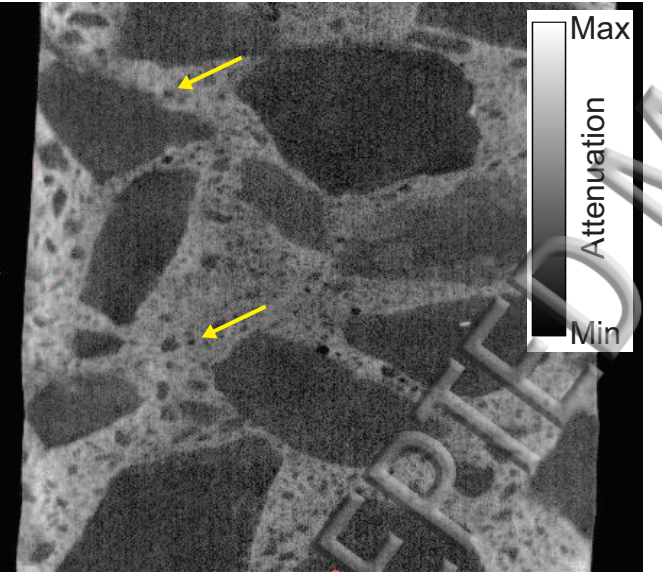




- 1 Thimble of Beam Tube
- 2 Tapered Collimator
- 3 Bismuth Filter
- 4 Aperture Selector
- 5 Rotating Drum Shutter
- 6 Wax and Shot Filled Shields
- 7 Evacuated Flight Tube
- 8 Sample Position
- 9 Neutron Detector
- 10 Neutron Beam Stop
- 11 X-ray Microfocus Tube
- 12 X-ray Detector







(a)

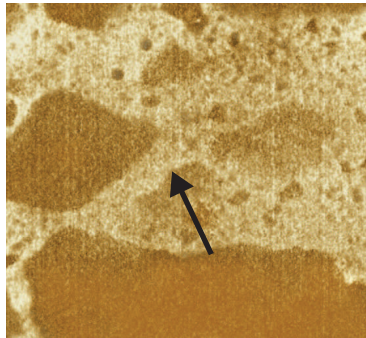


(b)



1 cm

(c)



(d)

